Dynamic Insight into the Interaction between Porphyrin and G-quadruplex DNAs: Time-Resolved Fluorescence Anisotropy Study

Guoqing Jia,[†,‡] Zhaochi Feng,[†] Chunying Wei,[†,§] Jun Zhou,[†,‡] Xiuli Wang,[†,‡] and Can Li*[,†]

State Key Laboratory of Catalysis, Dalian Institute of Chemical Physics, Chinese Academy of Sciences, Dalian 116023, China, and Graduate University of Chinese Academy of Sciences, Beijing 100049, China

Received: June 29, 2009; Revised Manuscript Received: September 28, 2009

Understanding the nature of the interaction between small molecules and G-quadruplex DNA is crucial for the development of novel anticancer drugs. In this paper, we present the first data on time-resolved fluorescence anisotropy study on the interaction between a water-soluble cationic porphyrin H_2TMPyP4 and four distinct G-quadruplex DNAs, that is, $AG_3(T_2AG_3)_3$, thrombin-binding aptamer (TBA), $(G_4T_4G_4)2$, and $(TG_4T)4$. The anisotropy decay curves show the monoexponential for free H_2TMPyP4 and the biexponential upon binding to the excess amount of G-quadruplex DNAs. The biexponential anisotropy decay can be well interpreted using a wobbling-in-the-cone model. The orientational diffusion of the bound H_2TMPyP4 is initially restricted to a limited cone angle within the G-quadruplex DNAs, and then an overall orientational relaxation of the G-quadruplex DNA-H_2TMPyP4 complexes occurs in a longer time scale. It was found that the dynamics of the restricted internal rotation of bound H_2TMPyP4 strongly depends on the ending structures of the G-quadruplex DNAs. According to the order parameter (Q) calculated from the wobbling-in-the-cone model, we deduce that the degree of restriction around the bound H_2TMPyP4 follows the order of TBA > $(TG_4T)4$ > $AG_3(T_2AG_3)_3$ > $(G_4T_4G_4)2$. Especially, based on the maximum order parameter (Q) of bound H_2TMPyP4 within TBA, a new sandwich-type binding mode for TBA-H_2TMPyP4 complex was proposed in which both terminal G-quartet and T•T base pair stack on the porphyrin ring through $\pi-\pi$ interaction. This study thus provides a new insight into the interaction between G-quadruplex DNAs and H_2TMPyP4.

1. Introduction

The guanine-rich single-stranded DNA can form G-quadruplex DNA.[1] Such sequences are found at the ends of chromosomes in the telomeric regions and in the transcriptional regulatory regions in several important oncogenes.[2−5] Compounds that bind and stabilize G-quadruplex DNAs can be potential candidates for antitumor drugs.[5−14] Therefore, studies of the G-quadruplex DNA-ligand binding interactions become an active topic of research.

The interaction of porphyrin derivative 5,10,15,20-tetrakis(*N*-methylpyridinium-4-yl) −21*H*,23*H*-porphyrin (H_2TMPyP4) (Scheme 1a) with G-quadruplex DNAs is a typical example and has been extensively studied by various biophysical methods,[5,15−24] UV−vis, fluorescence, and circular dichroism (CD) are common spectroscopic methods to provide useful information on the overall nature of the G-quadruplex DNA-H_2TMPyP4 complex, such as binding stoichiometry, binding affinity, and binding modes.[16−18,20,23,24] As a calorimetric technique, isothermal titration calorimetry (ITC) can provide quantitative information about the thermodynamics of G-quadruplex DNA-H_2TMPyP4 interaction.[16,18,24] NMR[5,20] and X-ray crystallography[22] can give a detailed structural information on G-quadruplex DNA-H_2TMPyP4 complex. In addition, molecular modeling and molecular dynamic studies are also important approaches for estimating the interaction energy and predicting the possible structure of the G-quadruplex DNA-H_2TMPyP4 complex.[15,18] It will be readily seen that all of above-mentioned techniques are characteristic of steady-state description about the G-quadruplex DNA-H_2TMPyP4 complex but less dynamic information. Recently, a surface plasmon resonance (SPR) spectroscopy has been used to investigate the kinetics of the G-quadruplex DNA-H_2TMPyP4 interaction in terms of association and dissociation rate constants.[24] However, to the best of our knowledge, there is no report on the dynamic description on the H_2TMPyP4 within G-quadruplex DNA as well as the overall dynamic property of the G-quadruplex-H_2TMPyP4 complex. It has been reported that long genome-derived DNA duplexes undergo collective long-range base-pair twisting along the long axis and bending motions along the short axis.[25−27] The dynamic dependence of the intercalated fluorophores on these long genome-drived DNA motions has been extensively studied.[25−30] Compared to the long genome-derived DNA duplexes, G-quadruplex DNA possesses substantially different topology due to its shorter strand, diverse loop structures, hoogsteen hydrogen bonding, base-stacking interaction, and metal ion coordination between G-tetrads.[2−4] Therefore, it will be interesting to investigate the dynamics of ligands interactions with G-quadruplex that have been, so far, poorly understood.

Time-resolved fluorescence anisotropy is a powerful tool to investigate the dynamic information on the reorientation of the fluorophore in the time scale of the fluorescence decay.[25−33] It has been widely used to probe the association of small ligands with macromolecules or macromolecule−macromolecule interactions.[31−33] Usually, both the global rotational motion of the target macromolecule and the local probe motion within the macro-

* To whom correspondence should be addressed. E-mail: canli@dicp.ac.cn. Tel: 86-411-84379070. Fax: 86-411-84694447. Web page: http://www.canli.dicp.ac.cn.

† Chinese Academy of Sciences.

‡ Graduate University of Chinese Academy of Sciences.

§ Present address: Key Laboratory of Chemical Biology and Molecular Engineering of Ministry of Education, Institute of Molecular Science, Shanxi University, Taiyuan 030006, China.

10.1021/jp906060d
Published on Web 11/19/2009

SCHEME 1: Structures of H_2TMPyP4 (a) and Schematic Diagrams of $AG_3(T_2AG_3)_3$ (b), TBA (c), $(G_4T_4G_4)2$ (d), and $(TG_4T)4$ (e) G-Quadruplex DNAs[a]

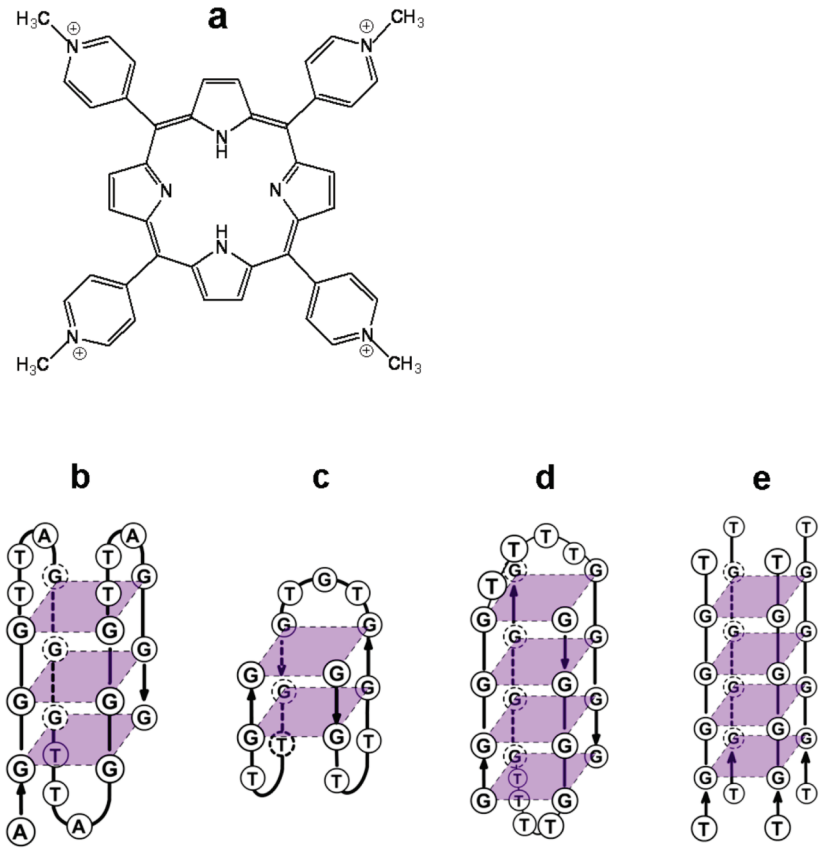

[a] Arrows denote 5′-3′ strand alignment for each DNA. The fitting metal ions (K^+ or Na^+) between the two G-quartets are omitted.

molecule can cause the fluorescence depolarization. Therefore, time-resolved fluorescence anisotropy measurement can provide the detailed information about the local dynamic processes within the biomolecular matrix and overall dynamic property of the biomolecules.[33]

It is well-known that the structureless fluorescence emission spectrum of free H_2TMPyP4 will be transformed into the two-band spectrum upon its binding to the G-quadruplex DNA.[16,17,23,24,34] This characteristic fluorescence behavior of H_2TMPyP4 can provide a good opportunity to investigate the interaction between G-quadruplex DNA and H_2TMPyP4 using time-resolved fluorescence anisotropy spectroscopic technique.

In this paper, the interactions of H_2TMPyP4 with four distinct G-quadruplex DNAs, that is, intramolecular basket-type $AG_3(T_2AG_3)_3$, intramolecular chair-type thrombin-binding aptamer (TBA), intermolecular dimer-hairpin-folded $(G_4T_4G_4)2$, and intermolecular parallel $(TG_4T)4$, have been studied for the first time using time-resolved fluorescence anisotropy spectroscopy. Contrary to the monoexponential fluorescence anisotropy decay of H_2TMPyP4 in a buffer medium, the biexponential anisotropy decay was found upon H_2TMPyP4 binding to excess amount of G-quadruplex DNAs. This biexponential anisotropy decay is well explained by the wobbling-in-the-cone model. The parameters obtained from the wobbling-in-the-cone model showed that the bound H_2TMPyP4 would execute distinct dynamic behavior toward the four G-quadruplex DNAs, which strongly depends on the ending structures of the four G-quadruplex DNAs. For TBA-H_2TMPyP4 complex, a new sandwich-type binding mode has also been proposed according to the anisotropy analysis.

2. Materials and Methods

2.1. Materials. The DNA oligonucleotides TG_4T, $G_4T_4G_4$, $G_2T_2G_2TGTG_2T_2G_2$, and $AG_3(T_2AG_3)_3$ were purchased from Shanghai Sangon Biological Engineering Techonology & Services Co., Ltd. (China). Single-strand concentrations were determined by measuring the absorbance at 260 nm in UV−vis spectra. Single-strand extinction coefficients were calculated by a nearest-neighbor approximation method,[35] using extinction coefficients at 260 nm of 57 800, 115 200, 143 300, and 228 500 $M^{-1}cm^{-1}$ for TG_4T, $G_4T_4G_4$, $G_2T_2G_2TGTG_2T_2G_2$ and $AG_3(T_2AG_3)_3$, respectively. The intra- and intermolecular G-quadruplexes were prepared as follows. The oligonucleotide samples were dissolved in a buffer solution consisting of 10 mM Tris-HCl, 1 mM Na_2EDTA, and 100 mM KCl for $(TG_4T)4$ and TBA or 100 mM NaCl for $(G_4T_4G_4)2$ and $AG_3(T_2AG_3)_3$ at pH 7.5. The mixture was then heated to 90 °C for 10 min, cooled down to room temperature (22 °C) with a cooling rate of around 0.5 °C/min, and then incubated at 4 °C for 12 h. The concentration of G-quadruplex DNA stock solution is 0.3 mM. The H_2TMPyP4 sample in the form of tetra-*p*-tosylate salt was purchased from Tokyo Kasei Kogyo Co., Ltd. (Japan). A 1 mM H_2TMPyP4 stock solution in Milli-Q water was stored in the dark at −20 °C to prevent the photodegradation. In the experiment, freshly diluted H_2TMPyP4 buffer solution (10 mM Tris-HCl, 1 mM Na_2EDTA, and 100 mM KCl or 100 mM NaCl, pH 7.5) with H_2TMPyP4 concentration of 4 μM was used. The concentration of H_2TMPyP4 was determined by measuring its absorbance at 424 nm in UV−vis spectra with an extinction coefficient of 2.26×10^5 M^{-1} cm^{-1}.[36] UV−vis spectra were

recorded on a Jasco-V550 UV−vis double-beam spectrophotometer with a 1 cm path length quartz cuvette.

2.2. Circular Dichroism Spectroscopy. CD experiments were performed at 22 °C using a Jasco-820 spectropolarimeter. Each measurement was recorded from 200 to 320 nm in a 1 cm path length quartz cuvette at a scanning rate of 50 nm/min. The final data were the average of three measurements. The concentration of G-quadruplex DNA is 9 μM. The scan of the buffer alone was used as the background, which was subtracted from the average scan for each sample.

2.3. Fluorescence Spectroscopy. All of the fluorescence experiments were carried out at 22 °C on a FLS920 fluorescence spectrometer (Edinburgh Instruments, U.K.) with a 1 cm path length quartz cuvette. G-quadruplex DNA-H_2TMPyP4 samples with different molar ratios were prepared by adding corresponding G-quadruplex DNA stock solution to the freshly diluted H_2TMPyP4 buffer solution (10 mM Tris-HCl, 1 mM Na_2EDTA, and 100 mM KCl or 100 mM NaCl, pH 7.5). In the final mixture, the concentration of H_2TMPyP4 was fixed at 4 μM.

2.3.1. Steady-State Fluorescence Emission Spectroscopy. The excitation wavelength was set at 430 nm and the emission spectrum was collected from 600 to 800 nm. Both excitation and emission slits were set at 2 nm. The integration time for 1 nm step was 1 s.

2.3.2. Time-Resolved Fluorescence Anisotropy Spectroscopy. Time-resolved fluorescence anisotropy spectra were recorded using the time-correlated single photon counting (TCSPC) method. The excitation source is a picosecond pulsed diode laser at 406.8 nm with pulse width of 64.2 ps. All decays were measured using a 4096-channel analyzer. The time resolution per channel was 24 ps. Data analysis was carried out on the commercial software provided by Edinburgh Instruments. The quality of the fit was evaluated using the reduced χ^2 as well as the visual inspection of the fit and the data.

Time resolved-fluorescence anisotropy ($r_i(t)$) is defined by the following expression:

$$r_i(t) = \frac{I_{VV_i}(t) - G_i I_{VH_i}(t)}{I_{VV_i}(t) + 2G_i I_{VH_i}(t)} \quad (1)$$

where $I_{VV_i}(t)$ and $I_{VH_i}(t)$ are the temporal emission intensities at parallel and perpendicular emission polarization with respect to vertical excitation polarization. G_i is the correction factor of the polarization bias of the instrument. The G_i is calculated as follows:

$$G_i = \frac{I_{HV_i}}{I_{HH_i}} \quad (2)$$

The G factor at a given fluorescence emission wavelength (i) was independently obtained by exciting the sample with a horizontally polarized excitation beam and collecting the two polarized fluorescence decays, one perpendicular and the other parallel to the horizontally polarized excitation beam.

The fluorescence anisotropy decay was analyzed according to

$$r(t) = \sum_i \beta_i \exp(-t/\phi_i) \quad (3)$$

where β_i is the limiting anisotropy of component i, and ϕ_i is the corresponding correlation time. The total limiting anisotropy is r_0, where $r_0 = \sum_i \beta_i$

3. Results and Discussion

3.1. Structural Characterization of G-Quadruplex DNAs. To avoid complexity from DNA structural diversity, the four G-quadruplex DNAs used in our experiment were carefully selected based on their well-established tertiary structures. Human telomere sequence $AG_3(T_2AG_3)_3$ folds intramolecularly into an antiparallel basket-type G-quadruplex DNA stabilized by three stacked G-tetrads that are connected by two lateral loops and a central diagonal loop in the presence of Na^+.[37] The NMR solution structure of TBA[38,39] indicates that it possesses an antiparallel chair-type structure with two guanine quartets connected by two T-T loops spanning the narrow grooves at one end and a T-G-T loop spanning a wide groove at the other end. In the case of *Oxytricha* telomere repeat sequence $G_4T_4G_4$, a dimer-hairpin-folded antiparallel G-quadruplex DNA is formed in the Na^+ buffer solution, which includes two equivalent diagonal TTTT loops across the diagonal of each end of G-quartet.[40,41] $(TG_4T)4$ forms stable parallel four-stranded G-quadruplex DNA in the presence of K^+.[42] Schematic description of four the G-quadruplex DNAs is shown in Scheme 1. CD data further confirm the formation of targeted G-quadruplex DNA structures. $AG_3(T_2AG_3)_3$ (Figure 1a), TBA (Figure 1b), and $(G_4T_4G_4)2$ (Figure 1c) are antiparallel G-quadruplex DNAs and present a positive peak at 295 nm and a negative peak at 263 nm.[43] Parallel four-stranded $(TG_4T)4$ (Figure 1d) exhibits a positive peak at 263 nm and a negative peak at 243 nm.[43]

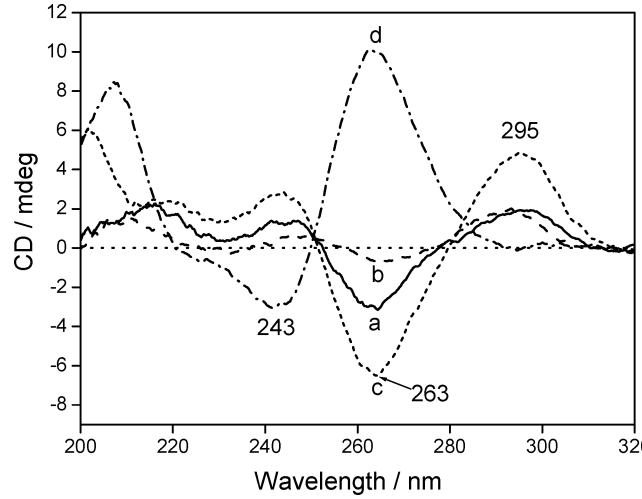

Figure 1. CD spectra of (a) $AG_3(T_2AG_3)_3$, (b) TBA, (c) $(G_4T_4G_4)2$, and (d) $(TG_4T)4$ G-quadruplex DNAs (9 μM) in buffer solution (pH 7.5).

3.2. Dynamic Insight into the Interaction of H_2TMPyP4 with G-Quadruplex DNAs. ***3.2.1. Homogeneous H_2TMPyP4 Population within G-Quadruplex DNA.*** Time-resolved fluorescence anisotropy has been established to be one of the most sensitive and powerful techniques to elucidate the dynamical information about the fluorophore in the confined environment. The interpretation of the fluorescence anisotropy decay is essentially based on an assumed model.[44] To have a model as simple as possible, the G-quadruplex DNA-H_2TMPyP4 complex with molar ratio of 10:1 was first selected to construct a homogeneous H_2TMPyP4 population. With the great excess of G-quadruplex DNAs, H_2TMPyP4 is expected to exclusively locate at the high affinity binding sites within the G-quadruplex DNA. Prior to the time-resolved fluorescence anisotropy measurement, the steady-state fluorescence emission spectra were recorded for H_2TMPyP4 and its four G-quadruplex DNA complexes (Figure 2). The fluorescence emission bands with maximum intensity were used for the monitoring wavelength for the time-resolved fluorescence anisotropy measurements.

Figure 3 shows the fluorescence anisotropy decays $r(t)$ of H_2TMPyP4 in a buffer solution and in different G-quadruplex DNAs surroundings. The data are analyzed with eq 3 and the

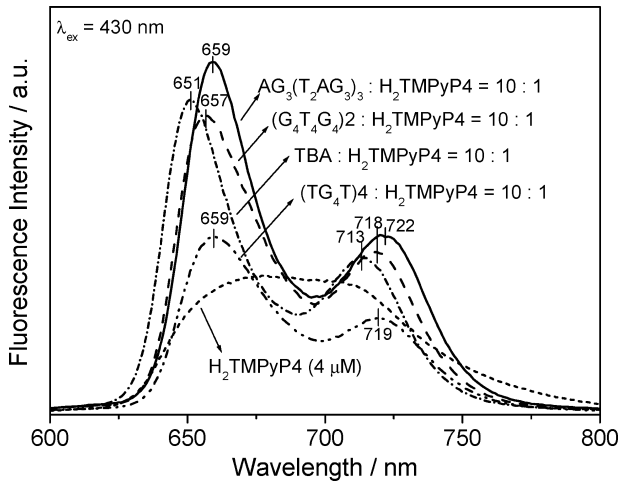

Figure 2. Steady-state fluorescence spectra of H_2TMPyP4 (4 μM) and its complexes with $AG_3(T_2AG_3)_3$, TBA, $(G_4T_4G_4)2$, and $(TG_4T)4$ G-quadruplex DNAs (40 μM) in buffer solution (pH 7.5).

corresponding anisotropy decay parameters are given in Table 1. The anisotropy decay of free H_2TMPyP4 (Figure 3a) is fitted by monoexponential function with the corresponding decay time of ca. 650 ps. Figure 3b−e shows the time-resolved fluorescence anisotropy decays of H_2TMPyP4 in $AG_3(T_2AG_3)_3$, TBA, $(G_4T_4G_4)2$, and $(TG_4T)4$ G-quadruplex DNAs. All G-quadruplex DNA-H_2TMPyP4 samples exhibit biexponential behavior with a faster anisotropy decay in the hundreds of picoseconds time scale and a relatively slower anisotropy decay in the order of nanosecond.

For the homogeneous H_2TMPyP4 population, the wobbling-in-the-cone model[45−47] can be used to explain the biexponential anisotropy decays for the G-quadruplex DNA-H_2TMPyP4 systems. A schematic representation is shown in Scheme 2. First, the faster rotational relaxation with a shorter correlation time (ϕ_1) is described as the motion of a restricted H_2TMPyP4, where the transition dipole moment can undergo orientational diffusion within a cone of semiangle θ. Second, the longer correlation time (ϕ_2) is ascribed to the slower overall orientational relaxation of G-quadruplex DNA-H_2TMPyP4 complex without any angular restriction. In this model, the anisotropy decay was fitted using the function

$$r(t) = r_0[Q^2 + (1 - Q^2)\exp(-t/\tau_c)]\exp(-t/\tau_m) \quad (4)$$

where Q is the generalized order parameter that characterizes the degree of restriction on the wobbling-in-the-cone orientational motion. The time constants τ_c and τ_m are the time scales for orientational motion in the cone and overall slower diffusion motion, respectively. In our analysis, the measured anisotropy for H_2TMPyP4 in G-quadruplex DNAs was fitted using the function

$$r(t) = \beta_1 \exp(-t/\phi_1) + \beta_2 \exp(-t/\phi_2) \quad (5)$$

The above function can be rearranged as follows:

$$r(t) = r_0[\beta_2/r_0 + \beta_1/r_0 \exp(-t/(\phi_1^{-1} - \phi_2^{-1})^{-1})] \times \exp(-t/\phi_2) \quad (6)$$

where $r_0 = \beta_1 + \beta_2$.

The physically meaningful model parameters (Q, τ_c and τ_m) can be calculated from the anisotropy decay parameters based on comparison of eqs 4 and 6

$$Q = (\beta_2/r_0)^{1/2} \quad (7)$$

$$\tau_c = (\phi_1^{-1} - \phi_2^{-1})^{-1} \quad (8)$$

$$\tau_m = \phi_2 \quad (9)$$

τ_m gives directly the orientational diffusion coefficient (D_m) of the angularly unrestricted orientation relaxation,[47]

$$D_m = \frac{1}{6\tau_m} \quad (10)$$

The calculated values of Q, τ_c, τ_m and D_m are summarized in Table 2.

In the simple case of spherical molecules, the relationship between the rotational time constant (τ_m) and the hydrodynamic volume (V) of a spherical rotating unit can be expressed by the Stokes−Einstein−Debye equation as follows:[33]

$$\tau_m = \frac{\eta V}{RT} \quad (11)$$

where η is the viscosity of the medium, R is the gas constant, and T is the temperature in Kelvin. The hydrodynamic volume of G-quadruplex DNA-H_2TMPyP4 complex is apparently higher than that of free H_2TMPyP4. Therefore, the value of τ_m shows a clear increase from 0.65 ns for free H_2TMPyP4 to 2.54−4.71 ns for G-quadruplex DNA-H_2TMPyP4 complexes. For the purpose of comparison among different G-quadruplex DNAs, the hydrodynamic volume of rotating unit is approximated to the molecular weight. The molecular weights of $AG_3(T_2AG_3)_3$, $(TG_4T)4$, and $(G_4T_4G_4)2$ are similar and about 1.5 times more than that of TBA. Thus, it is reasonable that the time constant of overall rotational diffusion motion (τ_m) of TBA-H_2TMPyP4 complex is higher than those in other G-quadruplex DNA-H_2TMPyP4 complexes.

In addition to overall rotational motion, the bound H_2TMPyP4 also reorients due to the restricted internal rotational motion. The order parameter, Q, is a measure of the time-averaged orientational distribution of the fluorescence probe in a confined space at equilibrium, which indicates the spatial constraint for the motion of the fluorescence probe inside the confined space.[46,47] For the fast unrestricted orientations, the value of the order parameter (Q) is zero; for the orientationally ordered systems, the Q value reaches the maximum of 1.0. The calculated values of the order parameter (Q) range from 0.53 to 0.80 for H_2TMPyP4 within different G-quadruplex DNAs, indicating a highly oriented distribution of H_2TMPyP4 in G-quadruplex DNAs. This is not surprising in view of the fact that the H_2TMPyP4 is confined within the G-quadruplex DNA binding site, which restricts the orientational freedom of the H_2TMPyP4 molecule. Further, the angular range of the restricted internal rotation of the H_2TMPyP4 within G-quadruplex DNAs was calculated using a model of isotropic diffusion within a cone. The cone semiangle θ can be obtained from the order parameter Q[45]

$$Q = \frac{\cos\theta(1 + \cos\theta)}{2} \quad (12)$$

The wobbling-in-the-cone diffusion constant D_c is given by[45]

$$D_c = \frac{(\cos\theta)^2(1+\cos\theta)^2\left(\ln\frac{1+\cos\theta}{2}+\frac{1-\cos\theta}{2}\right)}{\tau_c(1-Q^2)[2(\cos\theta-1)]} + \frac{(1-\cos\theta)[6+8\cos\theta-(\cos\theta)^2-12(\cos\theta)^3-7(\cos\theta)^4]}{24\tau_c(1-Q^2)} \quad (13)$$

The calculated values of θ and D_c are also listed in Table 2. It can be clearly seen that the calculated parameters (τ_c, D_c, Q, and θ) of H_2TMPyP4 internal motion are different from each other for four G-quadruplex DNAs.

It is widely accepted now that H_2TMPyP4 appears to bind by end-stacking on the G-quartet with high affinity.[5,9,10,15,17,19,20,23,24] Especially, the electrophoretic photocleavage assay provides the best experimental evidence for the end-stacking binding model.[19,20] Associated with four G-quadruplex DNAs in this experiment (Scheme 1), it is clear that end-stacking interaction mode is inevitably accompanied by some additional interaction from

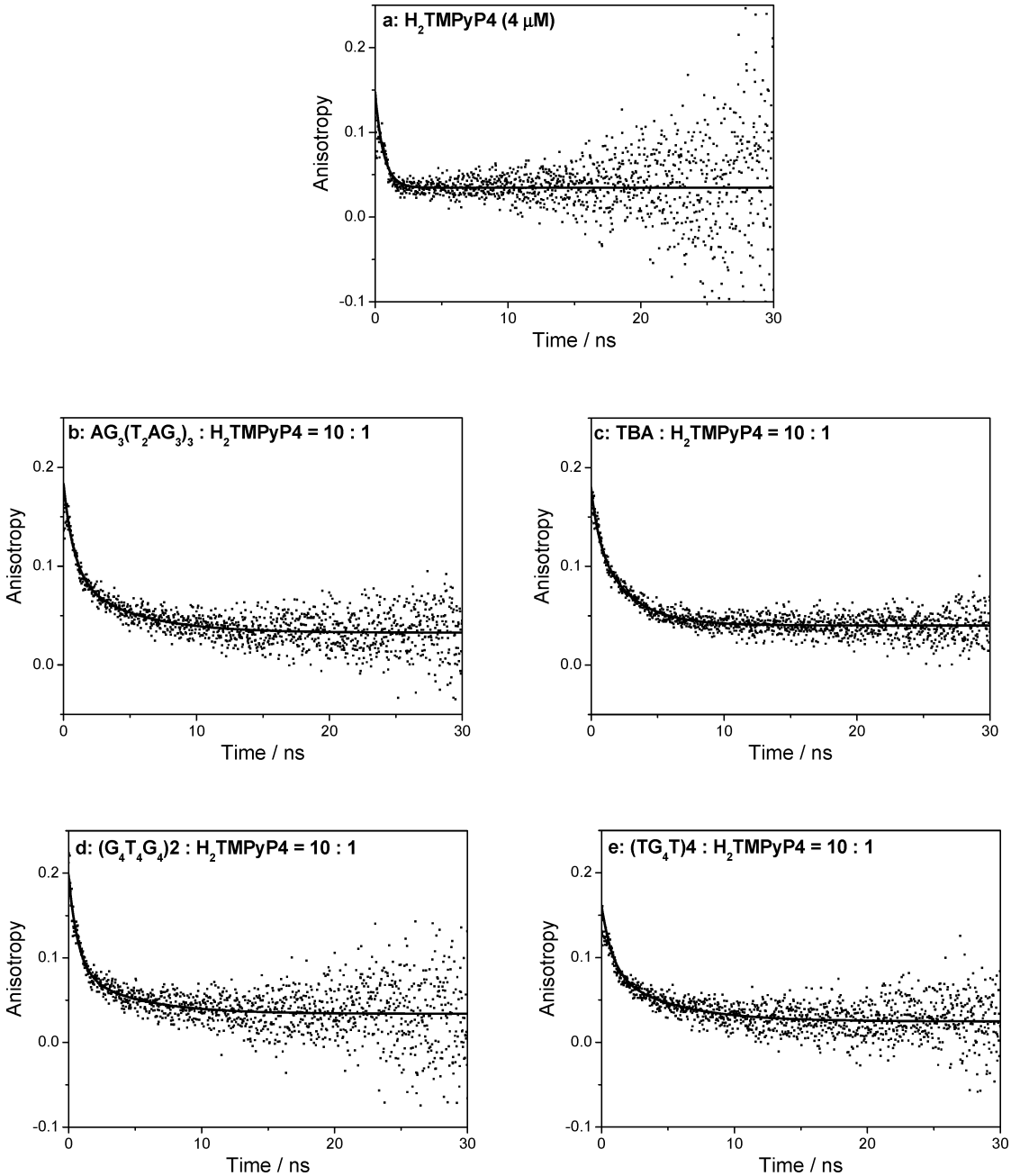

Figure 3. Time-resolved fluorescence anisotropy spectra of (a) H_2TMPyP4 (4 μM) and its complexes with (b) $AG_3(T_2AG_3)_3$, (c) TBA, (d) $(G_4T_4G_4)2$, and (e) $(TG_4T)4$ G-quadruplex DNAs (40 μM) in buffer solution (pH 7.5). Fitted curve is shown by the solid line.

TABLE 1: Fitted Parameters of Anisotropy Decays of H_2TMPyP4 and Its G-Quadruplex DNA Complexes

	sample	λ/nm	ϕ_1/ns	ϕ_2/ns	β_1	β_2	r_0	χ^2
1	H_2TMPyP4	676		0.65 ± 0.03		0.123 ± 0.006	0.123 ± 0.006	1.11
2	$AG_3(T_2AG_3)_3/H_2$TMPyP4 = 10:1	659	0.82 ± 0.08	4.71 ± 0.46	0.105 ± 0.006	0.061 ± 0.005	0.166 ± 0.011	0.99
3	TBA/H_2TMPyP4 = 10:1	651	0.57 ± 0.10	2.54 ± 0.16	0.058 ± 0.008	0.101 ± 0.010	0.159 ± 0.018	0.99
4	$(G_4T_4G_4)2/H_2$TMPyP4 = 10:1	657	0.71 ± 0.07	4.58 ± 0.67	0.138 ± 0.008	0.054 ± 0.006	0.192 ± 0.014	1.00
5	$(TG_4T)4/H_2$TMPyP4 = 10:1	659	0.83 ± 0.13	4.68 ± 0.52	0.076 ± 0.006	0.062 ± 0.006	0.138 ± 0.012	1.03

SCHEME 2: Schematic Representation of Time-Resolved Fluorescence Anisotropy of G-Quadruplex DNA-H_2TMPyP4 Complexes Using Wobbling-in-the-Cone Model

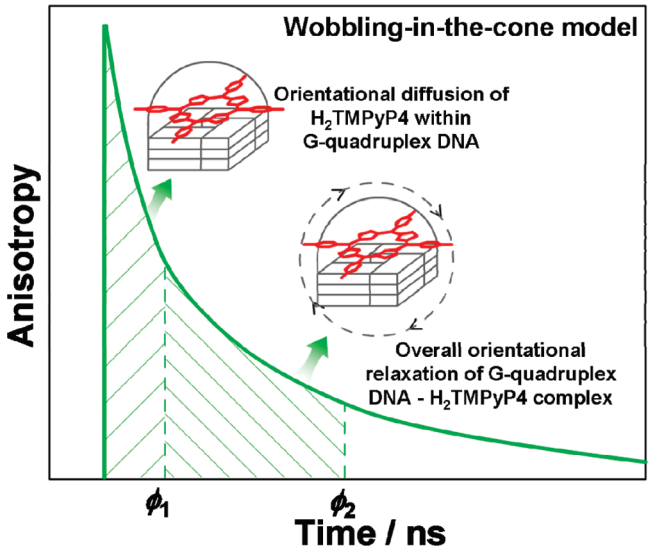

adjacent loops or terminal bases. Therefore, the diversiform ending structures in different G-quadruplex DNAs could be responsible for the different parameter values (τ_c, D_c, Q, and θ, Table 2) of the different G-quadruplex DNA-H_2TMPyP4 complexes.

The differences in the loop structures in terms of their length, base composition, and orientation in the G-quadruplex DNA can affect its molecular recognition by targeted molecules.[48,49] As shown in Scheme 1b, $AG_3(T_2AG_3)_3$ contains one diagonal TTA loop and two lateral TTA loops. The photocleavage experiment shows selective cleavage at the G-tetrad near the diagonal TTA, which strongly indicates that H_2TMPyP4 are end-stacking in diagonal TTA loop region[15,19,20] (Scheme 3a). $(G_4T_4G_4)2$ (Scheme 1d), a dimer-hairpin-folded G-quadruplex DNA, possesses two equivalent diagonal TTTT loops across the diagonal of each end G-quartet.[40] Therefore, it can be concluded that H_2TMPyP4 can accommodate itself in either of the diagonal TTTT loop regions (Scheme 3c). Compared to the diagonal TTA loop of $AG_3(T_2AG_3)_3$, the longer diagonal TTTT loop of $(G_4T_4G_4)2$ can make more space for H_2TMPyP4 to reside between the diagonal loop and the terminal G-tetrad. In addition, when H_2TMPyP4 locates in the diagonal TTTT loop region of $(G_4T_4G_4)2$ G-quadruplex DNA, the restrictive force mainly originates from the diagonal loop and the terminal G-quartet, whereas the regions beside the diagonal loop are relatively void. However, in the case of $AG_3(T_2AG_3)_3$, besides the restriction from the diagonal loop and the terminal G-quartet, the adenine at 5′ end also restricts the motion of the bound H_2TMPyP4. Therefore, it can be expected that the H_2TMPyP4 within $(G_4T_4G_4)2$ is less restricted than that within $AG_3(T_2AG_3)_3$. It can be seen from Table 2 that H_2TMPyP4 within $(G_4T_4G_4)2$ has smaller order parameter value ($Q = 0.53$), faster internal rotation time ($\tau_c = 0.84$ ns), bigger diffusion constant ($D_c = 2.03 \times 10^8$ s^{-1}) and broader angular range ($\theta = 50°$) of the restricted internal rotation compared to those for H_2TMPyP4 within $AG_3(T_2AG_3)_3$ ($Q = 0.61$, $\tau_c = 0.99$ ns, $D_c = 1.40 \times 10^8$ s^{-1} and $\theta = 44°$).

H_2TMPyP4 binds to the intermolecular parallel $(TG_4T)4$ G-quadruplex DNA through external stacking at the ends of G-quadruplexes[9,15,16] (Scheme 3d). In this binding model, the $\pi-\pi$ stacking interaction between the porphyrin ring and the G-quartet is predominant. Although there is no loop structure in this binding region, the H_2TMPyP4 is bounded by four thymines. This fence-type binding surrounding makes the internal rotation of H_2TMPyP4 to be more restricted than those of $(G_4T_4G_4)2$ and $AG_3(T_2AG_3)_3$. This can be quantitatively reflected by the bigger order parameter value ($Q = 0.67$), the slower internal rotation time ($\tau_c = 1.01$ ns), the smaller diffusion constant ($D_c = 1.18 \times 10^8$ s^{-1}), and the narrower angular range ($\theta = 40°$), as shown in Table 2.

TABLE 2: Calculated Parameters of Wobbling-in-the-Cone Model

	sample	τ_m/ns	D_m/s^{-1}	τ_c/ns	D_c/s^{-1}	Q	θ/°
1	H_2TMPyP4	0.65	2.56×10^8				
2	$AG_3(T_2AG_3)_3/H_2$TMPyP4 = 10:1	4.71	3.54×10^7	0.99	1.40×10^8	0.61	44
3	TBA/H_2TMPyP4 = 10:1	2.54	6.56×10^7	0.73	1.08×10^8	0.80	31
4	$(G_4T_4G_4)2/H_2$TMPyP4 = 10:1	4.58	3.64×10^7	0.84	2.03×10^8	0.53	50
5	$(TG_4T)4/H_2$TMPyP4 = 10:1	4.68	3.56×10^7	1.01	1.18×10^8	0.67	40

SCHEME 3: Schematic Depiction of End-Stacking Binding Mode of H_2TMPyP4 to G-Quadruplex DNAs[a]

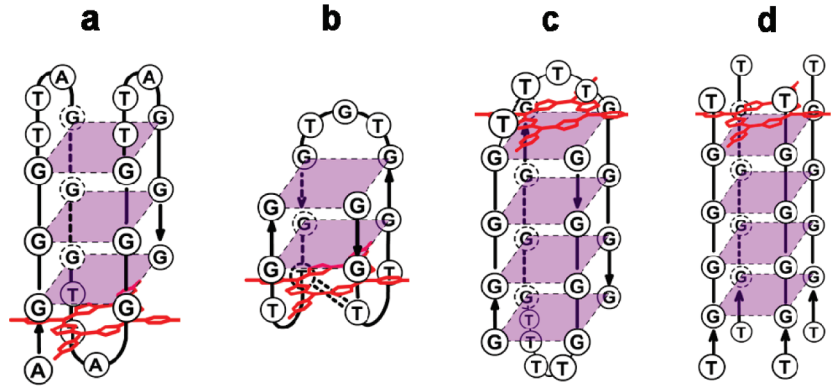

[a] (a) End-stacking on the G-quartet and overlapped with diagonal TTA loop of $AG_3(T_2AG_3)_3$, (b) sandwiching between G-quartet and T•T base pair at two TT loop region of TBA, (c) end-stacking on the G-quartet and overlapped with diagonal TTTT loop of $(G_4T_4G_4)2$ and (d) end-stacking on the G-quartet of $(TG_4T)4$. Arrows denote 5′-3′ strand alignment for each DNA. The fitting metal ions (K^+ or Na^+) between the two G-quartets are omitted.

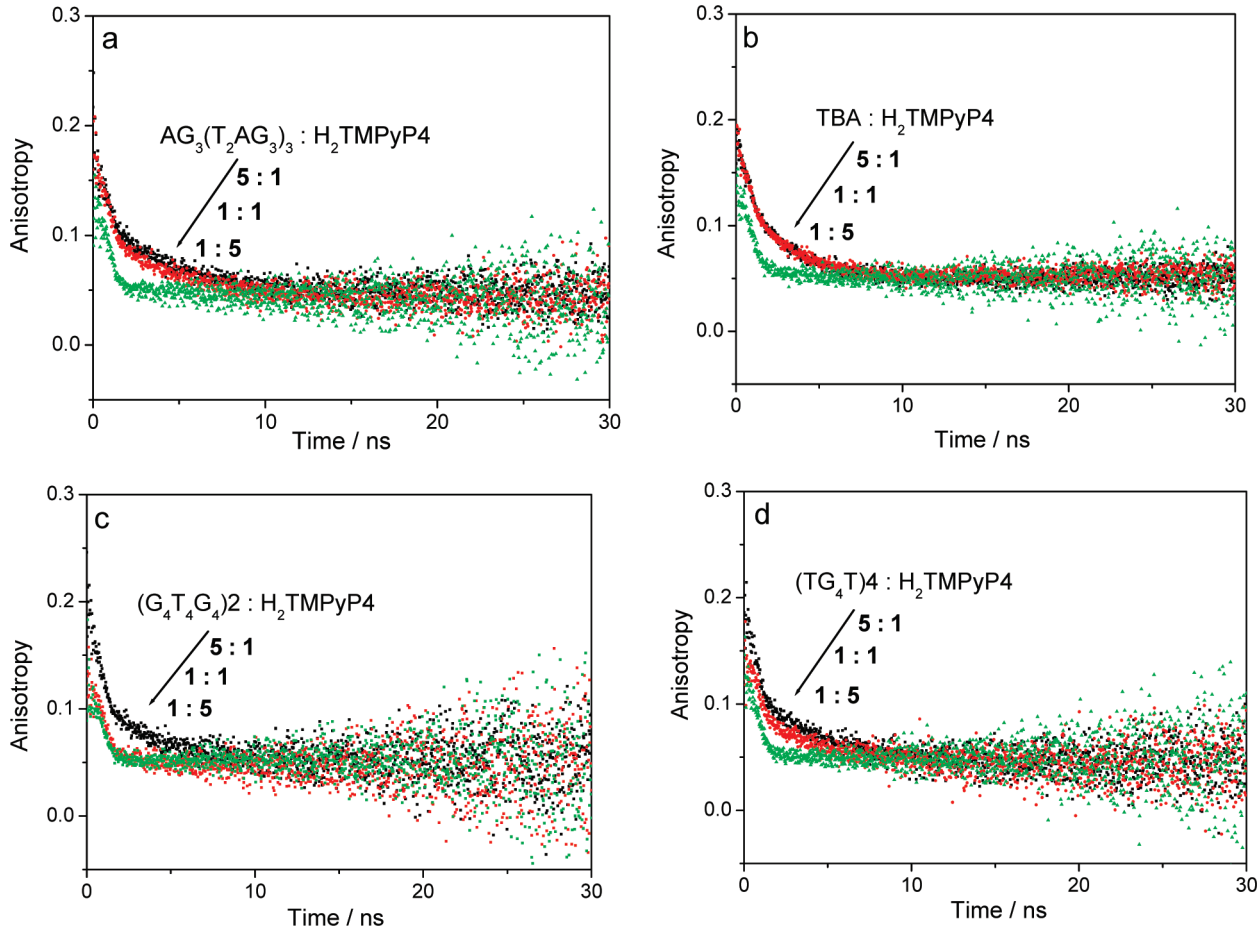

Figure 4. Time-resolved fluorescence anisotropy spectra of the G-quadruplex-H_2TMPyP4 complex with molar ratio of 5:1, 1:1, and 1:5.

From Table 2, the H_2TMPyP4 within TBA shows the maximum order parameter ($Q = 0.80$) among the four G-quadruplex DNAs. This is a clear indication that the bound H_2TMPyP4 has the least motional freedom at the TBA binding site. TBA is composed of two G-quartets connected by two TT loops at one end and a TGT loop at the other end (Scheme 1c). Han et al. predicted that one H_2TMPyP4 molecule would bind at the T-G quartet step of TBA instead of intercalation between the two G-quartets.[15] According to the G-quadruplex DNA-based aldol reaction, Tang et al. also suggested that the binding position of the H_2TMPyP4 is close to the two TT loops.[50] However, none of them provided the more detailed description of the binding site. For TT loop region, T•T base pair is formed between the two TT loops across the diagonal of the G-quartet and is stacked on the neighboring G-quartet.[38,39] Thus the T•T base pair could provide additional $\pi-\pi$ interaction to end-stacking H_2TMPyP4. In addition, it is reported that the G-quartet in proximity of the two TT loops appears more closely planar than the other G-quartet,[38] which might further enhance the $\pi-\pi$ interaction between bound porphyrin and G-quartet. Thus, within TT loop binding site, the H_2TMPyP4 is well protected from the water surrounding and the less polar environment may slow down the electronic mixing of S_1 and a close-lying CT state.[51,52] This conclusion is further supported by the results of the steady-state fluorescence results (Figure 2). As can be seen from Figure 2, the fluorescence intensity of H_2TMPyP4 within TBA are similar to those of $(G_4T_4G_4)2$ and $AG_3(T_2AG_3)_3$, but it is nearly twice more than that of $(TG_4T)4$. On the basis of the above analysis, we deduce that the H_2TMPyP4 is located at the TT loop region by sandwiching between T•T base pair and G-quartet through $\pi-\pi$ interaction (Scheme 3b). In this compact sandwich-type binding mode, the orientational diffusion of H_2TMPyP4 is severely restricted and thus results in the maximum order parameter ($Q = 0.80$), the smallest diffusion constant ($D_c = 1.08 \times 10^8\ s^{-1}$) and the narrowest angular range ($\theta = 31°$) among the four G-quadruplex DNAs (Table 2).

It should be noted that the internal rotation time constant (τ_c) of H_2TMPyP4 within TBA shows the minimum value among the four G-quadruplex DNAs, which is analogous to the case of overall rotational diffusion time constant (τ_m) of the TBA-H_2TMPyP4 complex. This implies that the internal rotation time constant (τ_c) is dependent on not only the local binding environment but also the hydrodynamic volume of the overall G-quadruplex DNA-H_2TMPyP4 complex. This can be ascribed to the shorter strand and further smaller hydrodynamic volume of the G-quadruplex DNA. For $AG_3(T_2AG_3)_3$, $(G_4T_4G_4)2$ and $(TG_4T)4$, similar hydrodynamic volume of these three G-quadruplex DNAs makes the τ_c be solely affected by the local binding microenvironement.

Interestingly, Haq et al. reported a binding affinity order of TBA > $(T_4G_4)4$ > $AG_3(T_2AG_3)_3$ for the H_2TMPyP4 according to isothermal titration calorimetry (ITC).[18] This sequence is in excellent agreement with our calculated order parameter (Q) from wobbling-in-the-cone model, where TBA > $(TG_4T)4$ > $AG_3(T_2AG_3)_3$. The more restrictive the binding mode is, the higher the binding affinity is. In this point, the wobbling-in-the-cone model used to interpret our time-resolved fluorescence anisotropy results is proved to be valid. Also, the order parameter (Q) could be used as an alternative parameter to evaluate the selectivity of the fluorescent drug for G-quadruplex DNA.

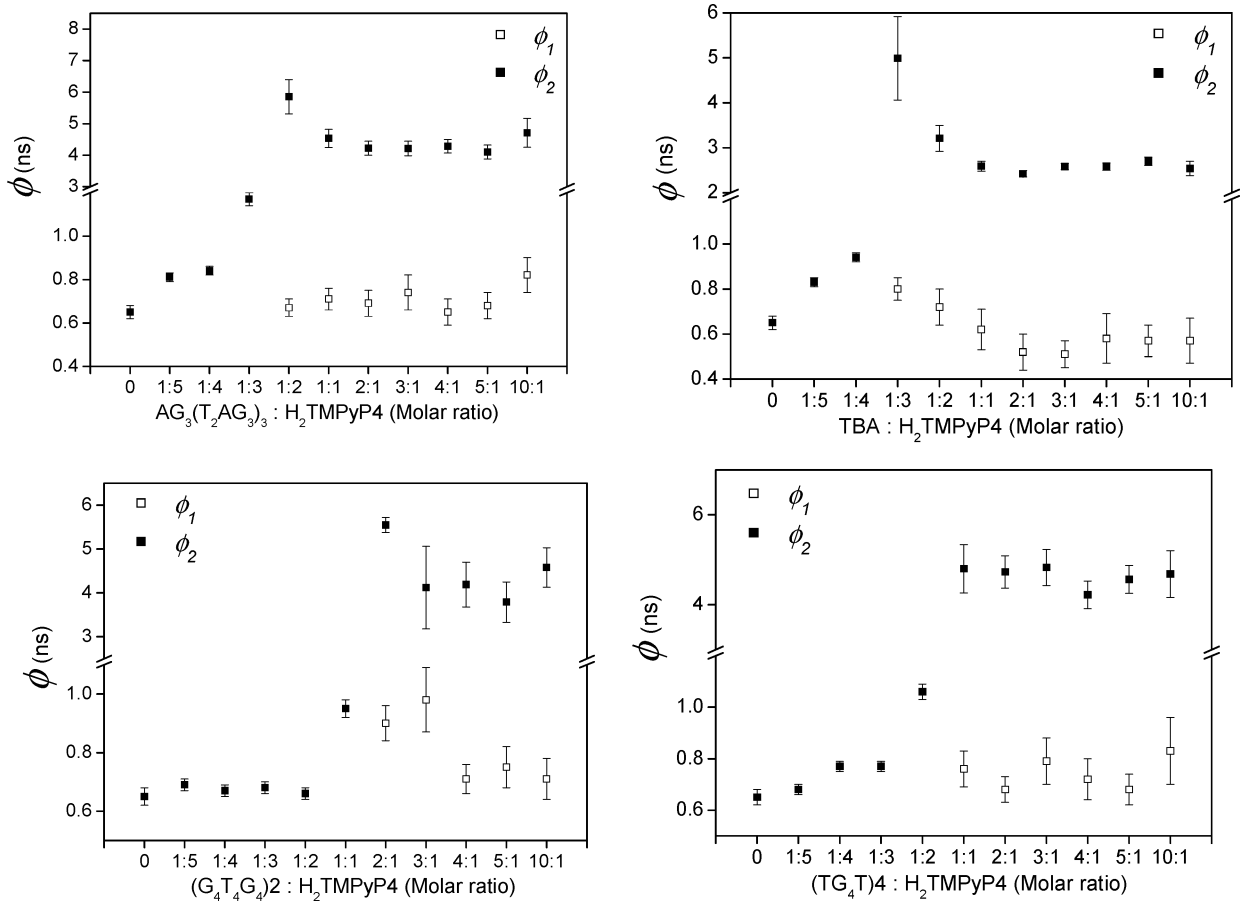

Figure 5. Fitted parameters of the time-resolved fluorescence anisotropy spectra using function of $r(t) = \beta_1 \exp(-t/\phi_1) + \beta_2 \exp(-t/\phi_2)$ for biexponential and $r(t) = \beta_2 \exp(-t/\phi_2)$ for monoexponential.

3.2.2. Transition from Homogeneous to Heterogeneous H_2TMPyP4 Population. Different G-quadruplex DNA/H_2TMPyP4 ratios around binding stoichiometry, that is, 5:1, 4:1, 3:1, 2:1, 1:1, 1:2, 1:3, 1:4, and 1:5, were also investigated by time-resolved fluorescence anisotropy spectroscopy. For the purpose of clarity, three representative decay curves (5:1, 1:1, and 1:5) of each G-quadruplex DNA-H_2TMPyP4 complex are displayed in Figure 4. All decay curves are analyzed with eq 3 and the detailed fitted results are summarized in Figure 5.

In the case of 2:1 ≤ [G-quadruplex DNA]/[H_2TMPyP4] ≤ 5:1, all decay curves are biexponential and the fitted parameters (ϕ_1, ϕ_2) show the similar values to the case of 10:1 (Figure 5). ϕ_2 of $(TG_4T)4$, $AG_3(T_2AG_3)_3$, and $(G_4T_4G_4)2$ show comparable values and are apparently higher than that of TBA (Figure S1 in Supporting Information). This is consistent with the results in the case of 10:1. Further, order parameter (Q) based on the wobbling-in-the-cone model are calculated and show the same order as the case of 10:1, that is, TBA > $(TG_4T)4$ > $AG_3(T_2AG_3)_3$ > $(G_4T_4G_4)2$ (Figure S2 in Supporting Information). Therefore, 2:1 ≤ [G-quadruplex DNA]/[H_2TMPyP4] ≤ 5:1, the bound H_2TMPyP4 still shows homogeneous population and the interaction between G-quadruplex DNA and H_2TMPyP4 can be well explained by the wobbling-in-the-cone model.

As shown in Figure 5, with decreasing of the molar ratio of G-quadruplex DNA to H_2TMPyP4, there is a clear transition around stoichiometry at 1:1 or 1:2. At this transition point, the fitted parameters (ϕ_1, ϕ_2) show great changes as compared to those above 2:1. In light of the two types of binding sites for H_2TMPyP4 within G-quadruplex DNA,[16,17,22−24] this transition might indicate the change from single binding site to the multiple binding sites, that is, from homogeneous H_2TMPyP4 population to heterogeneous H_2TMPyP4 population. At the molar ratio of G-quadruplex DNA/H_2TMPyP4 less than binding stoichiometry, the population of H_2TMPyP4 becomes more complex, including free H_2TMPyP4 and H_2TMPyP4 in different binding sites within G-quadruplex DNA. The approximate analysis based on eq 3 together with its corresponding wobbling-in-the-cone model is no longer valid.

In the heterogeneous probe population, the anisotropy decay is represented by[31−33]

$$r(t) = \sum_m f_m(t) r_m(t) \tag{14}$$

where

$$f_m(t) = \frac{\alpha_m \exp(-t/\tau_m)}{\sum_m \alpha_m \exp(-t/\tau_m)}$$

is the fraction of fluorescence at time t of m species; $r_m(t)$ describes the anisotropy decay of the m species.

According to the eq 14, in the case of heterogeneous probe population, the defined description of each species in terms of its own fluorescence (τ_m) and anisotropy ($r_m(t)$) property is prerequisite for the anisotropy decay analysis. However, it is difficult to get the individual fluorescence or anisotropy information on the weak binding H_2TMPyP4 within G-quadruplex DNA, which makes the anisotropy analysis more complicated.

4. Conclusion

This paper presents a comprehensive study on the dynamics of the interaction between H_2TMPyP4 and four G-quadruplex DNAs by time-resolved fluorescence anisotropy spectroscopic method. In the presence of excess amount of G-quadruplex DNA, the dynamics of H_2TMPyP4 can be well described using wobbling-in-the-cone model that involves fast orientational diffusion of bound H_2TMPyP4 within G-quadruplex DNA followed by slower, full orientational relaxation of the whole G-quadruplex DNA-H_2TMPyP4 complexes. According to the calculated parameters (τ_c, D_c, Q, and θ), it is deduced that the dynamics of the restricted internal rotation of H_2TMPyP4 strongly depends on the structures of the G-quadruplex DNAs, mainly originating from the different ending structures (loops and ending bases) at the H_2TMPyP4 binding site. A new binding mode of H_2TMPyP4 within TBA G-quadruplex DNA is proposed, where H_2TMPyP4 is in a sandwich form between T•T base pair and G-quartet. Our results demonstrate that time-resolved fluorescence anisotropy is an alternative method to investigate the interaction of G-quadruplex DNA with fluorescent drugs and also strongly indicate that the different loop topologies are critical to rational design of the ligands for targeting individual G-quadruplex DNA.

Acknowledgment. This work was supported by the National Natural Science Foundation of China (Grants 20621063, 20773123, and 20673110).

Supporting Information Available: This material is available free of charge via the Internet at http://pubs.acs.org.

References and Notes

(1) Davis, J. T. *Angew. Chem., Int. Ed.* **2004**, *43*, 668.
(2) Cech, T. R. *Angew. Chem., Int. Ed.* **2000**, *39*, 34.
(3) Neidle, S.; Parkinson, G. N. *Curr. Opin. Struct. Biol.* **2003**, *13*, 275.
(4) Huppert, J. L.; Balasubramanian, S. *Nucleic Acids Res.* **2007**, *35*, 406.
(5) Phan, A. T.; Kuryavyi, V.; Gaw, H. Y.; Patel, D. J. *Nat. Chem. Biol.* **2005**, *1*, 167.
(6) Mergny, J.-L.; Hélène, C. *Nat. Med.* **1998**, *4*, 1366.
(7) Han, H.; Hurley, L. H. *Trends Pharmacol. Sci.* **2000**, *21*, 136.
(8) Hurley, L. H. *Nat. Rev. Cancer* **2002**, *2*, 188.
(9) Neidle, S.; Parkinson, G. *Nat. Rev. Drug Discovery* **2002**, *1*, 383.
(10) Oganesian, L.; Bryan, T. M. *BioEssays* **2007**, *29*, 155.
(11) Patel, D. J.; Phan, A. T.; Kuryavyi, V. *Nucleic Acids Res.* **2007**, *35*, 7429.
(12) Monchaud, D.; Teulade-Fichou, M.-P. *Org. Biomol. Chem.* **2008**, *6*, 627.
(13) Balasubramanian, S.; Neidle, S. *Curr. Opin. Chem. Biol.* **2009**, *13*, 345.
(14) Ou, T.-M.; Lu, Y.-J.; Tan, J.-H.; Huang, Z.-S.; Wong, K.-Y.; Gu, L.-Q. *ChemMedChem* **2008**, *3*, 690.
(15) Han, H.; Langley, D. R.; Rangan, A.; Hurley, L. H. *J. Am. Chem. Soc.* **2001**, *123*, 8902.
(16) Freyer, M. W.; Buscaglia, R.; Kaplan, K.; Cashman, D.; Hurley, L. H.; Lewis, E. A. *Biophys. J.* **2007**, *92*, 2007.
(17) Zhang, H. J.; Wang, X. F.; Wang, P.; Ai, X. C.; Zhang, J. P. *Photochem. Photobiol. Sci.* **2008**, *7*, 948.
(18) Haq, I.; Trent, J. O.; Chowdhry, B. Z.; Jenkins, T. C. *J. Am. Chem. Soc.* **1999**, *121*, 1768.
(19) Han, F. X.; Wheelhouse, R. T.; Hurley, L. H. *J. Am. Chem. Soc.* **1999**, *121*, 3561.
(20) Wheelhouse, R. T.; Sun, D.; Han, H.; Han, F. X.; Hurley, L. H. *J. Am. Chem. Soc.* **1998**, *120*, 3261.
(21) Siddiqui-Jain, A.; Grand, C. L.; Bearss, D. J.; Hurley, L. H. *Proc. Natl. Acad. Sci. U.S.A.* **2002**, *99*, 11593.
(22) Parkinson, G. N.; Ghosh, R.; Neidle, S. *Biochemistry* **2007**, *46*, 2390.
(23) (a) Wei, C. Y.; Jia, G. Q.; Yuan, J. L.; Feng, Z. C.; Li, C. *Biochemistry* **2006**, *45*, 6681. (b) Wei, C. Y.; Jia, G. Q.; Zhou, J.; Han, G. Y.; Li, C. *Phys. Chem. Chem. Phys.* **2009**, *11*, 4025. (c) Wei, C. Y.; Han, G. Y.; Jia, G. Q.; Zhou, J.; Li, C. *Biophys. Chem.* **2008**, *137*, 19. (d) Wei, C. Y.; Wang, L. H.; Jia, G. Q.; Zhou, J.; Han, G. Y.; Li, C. *Biophys. Chem.* **2009**, *143*, 79.
(24) Arora, A.; Maiti, S. *J. Phys. Chem. B* **2008**, *112*, 8151.
(25) Allison, S. A.; Schurr, J. M. *Chem. Phys.* **1979**, *41*, 35.
(26) Barkley, M. D.; Zimm, B. H. *J. Chem. Phys.* **1979**, *70*, 2991.
(27) Millar, D. P.; Robbins, R. J.; Zewail, A. H. *J. Chem. Phys.* **1982**, *76*, 2080.
(28) Wahl, Ph.; Paoletti, J.; Le Pecq, J.-B. *Proc. Natl. Acad. Sci. U.S.A.* **1970**, *65*, 417.
(29) Millar, D. P.; Robbins, R. J.; Zewail, A. H. *Proc. Natl. Acad. Sci. U.S.A.* **1980**, *77*, 5593.
(30) Hogan, M.; Wang, J.; Austin, R. H.; Monitto, C. L.; Hershkowitz, S. *Proc. Natl. Acad. Sci. U.S.A.* **1982**, *79*, 3518.
(31) Bailey, M. F.; Thompson, E. H. Z.; Millar, D. P. *Methods* **2001**, *25*, 62.
(32) Guest, C. R.; Hochstrasser, R. A.; Allen, D. J.; Benkovic, S. J.; Millar, D. P.; Dupuy, C. G. *Biochemistry* **1991**, *30*, 8759.
(33) Lakowicz, J. R. *Principles of Fluorescence Spectroscopy*, 3rd ed.; Plenum: New York, 2006.
(34) Arthanari, H.; Basu, S.; Kawano, T.; Bolton, P. H. *Nucleic Acids Res.* **1998**, *26*, 3724.
(35) Cantor, C. R.; Warshaw, M. W.; Shapiro, H. *Biopolymers* **1970**, *9*, 1059.
(36) Pasternack, R. F.; Gibbs, E. J.; Villafranca, J. J. *Biochemistry* **1983**, *22*, 2406.
(37) Wang, Y.; Patel, D. J. *Structure* **1993**, *1*, 263.
(38) Schultze, P.; Macaya, R. F.; Feigon, J. *J. Mol. Biol.* **1994**, *235*, 1532.
(39) Macaya, R. F.; Schultze, P.; Smith, F. W.; Roe, J. A.; Feigon, J. *Proc. Natl. Acad. Sci. U.S.A.* **1993**, *90*, 3745.
(40) Smith, F. W.; Feigon, J. *Nature* **1992**, *356*, 164.
(41) Smith, F. W.; Feigon, J. *Biochemistry* **1993**, *32*, 8682.
(42) Aboul-ela, F.; Murchie, A. I. H.; Norman, D. G.; Lilley, D. M. J. *J. Mol. Biol.* **1994**, *243*, 458.
(43) Paramasivan, S.; Rujan, I.; Bolton, P. H. *Methods* **2007**, *43*, 324.
(44) Rachofsky, E. L.; Laws, W. R.; Michael, L. J.; Ludwig, B. *Methods Enzymol.* **2000**, *321*, 216.
(45) (a) Lipari, G.; Szabo, A. *Biophys. J.* **1980**, *30*, 489. (b) Tan, H.-S.; Piletic, I. R.; Fayer, M. D. *J. Chem. Phys.* **2005**, *122*, 174501.
(46) Maiti, N. C.; Mazumdar, S.; Periasamy, N. *J. Phys. Chem.* **1995**, *99*, 10708.
(47) Quitevis, E. L.; Marcus, A. H.; Fayer, M. D. *J. Phys. Chem.* **1993**, *97*, 5762.
(48) Campbell, N. H.; Patel, M.; Tofa, A. B.; Ghosh, R.; Parkinson, G. N.; Neidle, S. *Biochemistry* **2009**, *48*, 1675.
(49) Parkinson, G. N.; Cuenca, F.; Neidle, S. *J. Mol. Biol.* **2008**, *381*, 1145.
(50) Tang, Z.; Gonçlves, D. P. N.; Wieland, M.; Marx, A.; Hartig, J. S. *ChemBioChem* **2008**, *9*, 1061.
(51) Lang, K.; Mosinger, J.; Wagnerová, D. M. *Coord. Chem. Rev.* **2004**, *248*, 321.
(52) Vergeldt, F. J.; Koehorst, R. B. M.; Hoek, A. v.; Schaafsma, T. J. *J. Phys. Chem.* **1995**, *99*, 4397.

JP906060D